EXPERIMENTAL CHARACTERISATION AND MODELLING OF NON-LINEAR STRESS-STRAIN BEHAVIOUR AND STRAIN RATE EFFECTS FOR UNIDIRECTIONAL CARBON-EPOXY

H. Koerber[a*], M. Vogler[b], P. Kuhn[a], P.P. Camanho[c]

[a]*Institute for Carbon Composites, Faculty of Mechanical Engineering, Technische Universitaet Muenchen, Boltzmannstrasse 15, 85748 Garching bei München, Germany*
[b]*Matthias Vogler Engineering&Consulting Services, Sauerweinstr. 3, 30167 Hannover, Germany*
[c]*DEMec, Faculdade de Engenharia, Universidade do Porto, Rua Dr. Roberto Frias, 4200-465 Porto, Portugal*
**koerber@lcc.mw.tum.de*

Keywords: Strain rate effects, plasticity, failure envelopes, constitutive modelling

Abstract
The mechanical response of IM7-8552 was investigated for transverse tension and transverse tension / in-plane shear loading at static and dynamic strain rates using transverse tension and off-axis tension specimens. The dynamic tests were carried out on a split-Hopkinson tension bar at axial strain rates of 100 s^{-1}, using high speed photography and digital image correlation during the data reduction. From the measured axial strengths the failure envelope for the combined stress state was derived for both strain rates and compared with the Puck IFF Mode A failure criterion. The measured axial stress-strain response was simulated using a fully 3D transversely isotropic elastic-viscoplastic constitutive model. A very good correlation between the measured and numerically predicted stress-strain response was achieved for all specimen types and strain rate regimes.

1. Introduction

With the recently increased applications of fibre reinforced polymer matrix composites (FRPMCs) in primary automotive (BMW project i) and aeronautical structures (Airbus A350 and Boeing 787), the interest in an improved understanding of the mechanical behaviour of FRPMCs under high speed loading events such as crash or foreign object impact is remaining strong. Material behaviour such as plasticity and strain rate dependency should be considered for an accurate description of the energy dissipation when modelling the progressive failure of polymer composites under such loading events. Particularly in the light that composites with more damage tolerant toughened epoxy or thermoplastic resin systems are gaining in importance, which show pronounced non-linear stress-strain behaviour and strain rate dependency.

In the experimental part of this work the mechanical response of a unidirectional (UD) carbon-epoxy composite is investigated under transverse tension and combined transverse tension / in-plane shear loading at quasi-static and dynamic strain rates. The work is similar to the experimental investigations of Taniguchi et al. [1]. Together with previously published experimental data of static and dynamic off-axis compression tests, using the same material

system as in the present study [2], a comprehensive data set now exists however for the validation of numerical material models.

In the numerical part of this work the available tension tests are simulated using a fully 3D transversely isotropic elastic-viscoplastic constitutive model, able to predict the experimentally observed nonlinearities under multi-axial loading conditions prior to the onset of cracking [3].

2. Material and Experimental Setup

The UD prepreg system HexPly® IM7-8552 was used for this study. A UD panel with a thickness of 1.5mm was manufactured on a hot press, following the curing cycle as specified in the material data sheet. From the 1.5 mm panel rectangular 15°, 30° and 45° off-axis tension and 90° transverse tension specimens (Figure 1a) were cut on a water-cooled diamond saw. All specimens were glued into slotted steel adapters using the structural adhesive 3M Scotch-Weld™ DP490. An assembled specimen is shown in Figure 1b. It is noted that for the 30° and 45° off-axis tension and for the 90° transverse tension specimen the free specimen section, measured between the ends of the adapters, was set to be 20 mm. For the 15° off-axis tension specimen a free section of 30 mm was chosen to obtain a section where no fibre is attached to either of the two adapters.

The slotted adapters are required to attach the specimens to the split-Hopkinson tension bar apparatus. Therefore the specimen design was dictated by the specimen and attachment system needed for the dynamic tests. To allow a direct comparison between the static and dynamic tests, the same specimen types were used for the quasi-static reference tests.

The quasi-static test setup, using threaded adapters to attach the assembled specimen is shown in Figure 1c. A standard electro-mechanical test machine of the type Hegewald & Peschke Inspect Table 100 was used. The specimens were loaded at a constant displacement rate of 0.5 mm.min^{-1}, which results in a strain rate of $\dot{\varepsilon} \approx 4 \times 10^{-4}$ s^{-1}. The 3D in-plane strain field in the free specimen section was measured using the DIC system ARAMIS-4M.

The dynamic tests were performed on a split-Hopkinson tension bar as illustrated in Figure 2. The apparatus consists of titanium ∅20 mm loading-, ∅16 mm incident- and ∅16 mm transmission-bars with lengths of 2.15, 3 and 1.8 m, respectively.

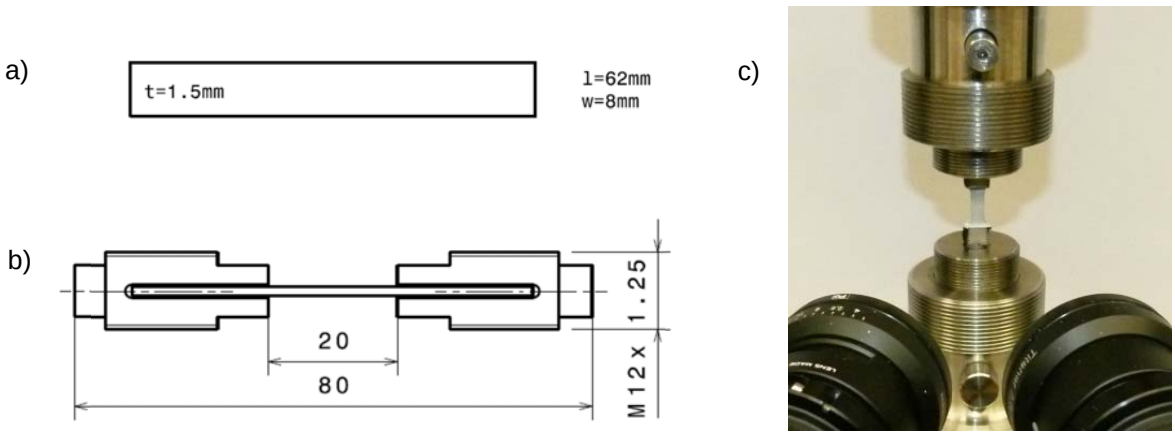

Figure 1. Off-axis tension specimen (a), transverse tension specimen (b), off-axis tension specimen glued into slotted adapters (c) and quasi-static test setup (d).

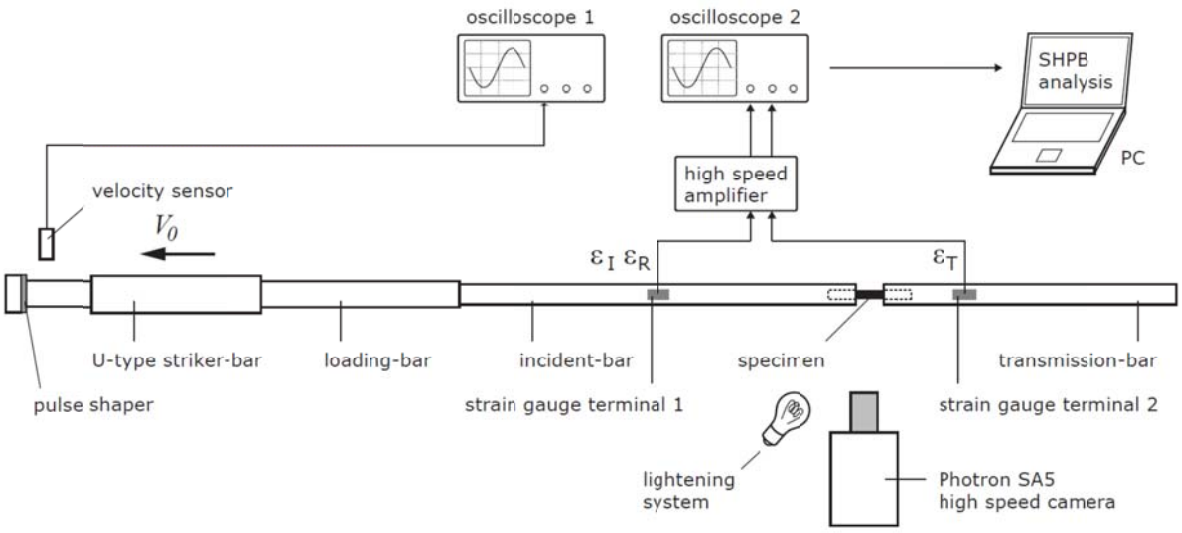

Figure 2. Split-Hopkinson tension bar setup for dynamic tests (striker-bar acceleration system not shown).

The split-Hopkinson tension bar design is based on a novel concept proposed by [4], utilizing a U-shaped striker bar. In the present work a 0.5 m long titanium stiker-bar was used. The deformation of the tensile specimen was monitored by a Photron SA5 high speed camera, allowing the determination of the 2D in-plane strain field also using the DIC system ARAMIS. Camera frame rate and resolution were set to 100000 fps and 448 × 136 pixels^2.

Due to the low plastic strains observed for the static tests, predominantly linear specimen stress-strain behaviour was expected to occur for the dynamic tests. Hence all tests on the Hopkinson bar were performed with ramp-shaped incident pulses, which had proven to be ideally suited to obtain constant strain rates for a linear specimen material behaviour in a previous study [5]. The pulse shaper consisted of a ring of 2mm thick silicon rubber wrapped around the impact flange at the end of the loading bar.

3. Data Reduction

For the static tests the axial specimen stress was determined by dividing the load-signal by the specimen cross-section, while the axial strain was determined from the DIC measurement by averaging the axial strain field over an area of 5 × 5 mm² in the specimen centre.

For the dynamic tests the axial specimen stress-time signal was calculated from the transmitted bar strain-wave using standard split-Hopkinson pressure bar analysis (SHPBA), while the axial specimen strain was determined from the dynamic DIC measurements, again averaging the axial strain field over an area of 5 × 5 mm². The data reduction procedure for the dynamic tests is therefore the same as described in [2].

From the static and dynamic axial stress-strain curves of the off-axis tension tests, the experimental failure envelope for combined transverse tension and in-plane shear loading was constructed by transforming the axial strengths into the material coordinate system. Due to the low failure strains and the boundary conditions of the tensile specimens, significant fibre rotation, as observed when performing off-axis compression tests [2], was not measured this time and was therefore not considered in the transformation.

4. Experimental Results

The axial stress-strain curves of the off-axis tension and transverse tension specimens for static and dynamic loading are presented together with the results of the numerical model (Section 5) in Figure 6 (Section 6). For each specimen type and strain rate regime three tests were performed. For the 45° off-axis tension specimen type only one stress-strain curve is shown for each strain rate regime since the other specimens did not produce a valid failure mode (failure in the free specimen section). Also, at the time of writing results from dynamic transverse tension tests were not yet available and are therefore not included in Figure 6d.

While the quasi-static transverse tension specimen type shows a linear stress-strain response up to failure, all quasi-static off-axis tension tests reveal a non-linear stress-strain response. Under dynamic loading, at an axial strain rate of $\dot{\varepsilon} = 100$ s^{-1}, the stress-strain curves are becoming more linear and the measured axial strength increases by 47%, 30% and 24% for the 15°, 30° and 45° off-axis specimen type, respectively. No significant strain rate effect was measured for the axial modulus of elasticity.

Figure 3a shows the complete envelope for inter-fibre failure (IFF) of IM7-8552 under static and dynamic loading. The data points for combined transverse tension / in-plane shear loading were generated from the herein presented axial stress-strain curves (Figure 6), while the data for the combined transverse compression / in-plane shear stress state as well as the pure in-plane shear strengths, were taken from [2]. In addition, the static and dynamic failure envelopes as defined by the 2d Puck IFF failure criteria [6] were included.

Considering the difference in the specimen design, the different static and dynamic test setups and laboratories used for the off-axis compression tests [2] and the presented off-axis tension tests, a very good match was achieved for the experimental compressive and tensile data sets. It is therefore concluded that the material behaviour of IM7-8552 for the investigated combined stress states and strain rate regimes is well captured.

Figure 3b shows enlarged the stress space for combined transverse tension / in-plane shear loading. For quasi-static strain rates it is seen that the experimental and the predicted failure envelopes correlate very well. The Puck Mode A failure envelope for dynamic loading was constructed, assuming a 40% increase of the transverse tensile strength, which corresponds to the strain rate effect observed for the failure envelope under combined transverse compression / in-plane shear loading [2].

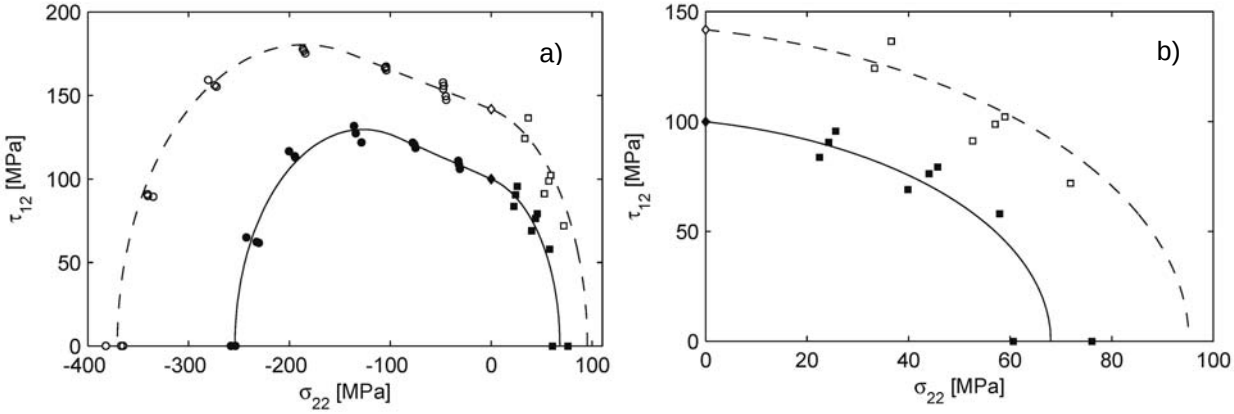

Figure 3. Experimental and predicted inter-fibre failure (IFF) envelope for IM7-8552 loaded at static ($\approx 4 \times 10^{-4}$ s^{-1}) and dynamic (tension: ≈ 100 s^{-1}, compression: 100 – 350 s^{-1}) axial strain rates.

For the 15° off-axis tension specimen again a very good correlation between experimental and predicted failure was obtained. For the 30° and the 45° specimen type the predicted dynamic failure appears to be slightly over-predictive. A possible explanation for this observation may be as follows.

All dynamic off-axis tension tests were performed at a constant axial strain rate of 100 s^{-1}. For the in-plane shear dominated 15° off-axis tension specimen the shear strain rate, acting in the failure plane, is approx. 350 s^{-1}, which is similar to the shear strain rate observed for the dynamic 15° off-axis compression tests [2]. As the off-axis angle is increased to 30° and 45° the strain rate acting on the failure plane is gradually reduced. Therefore to obtain a constant strain rate with respect to the shift from an in-plane shear to a transverse tensile material response, the axial strain rate needs to be increased accordingly.

5. Numerical Model

Hereafter, the constitutive model used for the prediction of the off-axis tensile tests is briefly presented. This model represents a viscoplastic extension of the transversely isotropic elastic-plastic model presented in [3]. The main objective is the prediction of the pressure dependent pre-failure nonlinearities under multiaxial loading conditions as they are observed in carbon epoxy composites. The material model proposed consists of an elastic-viscoplastic model, assuming the additive decomposition of the strain tensor ($\boldsymbol{\varepsilon}$) into the elastic ($\boldsymbol{\varepsilon}^{e}$) and the viscoplastic parts ($\boldsymbol{\varepsilon}^{vp}$):

$$\boldsymbol{\varepsilon} = \boldsymbol{\varepsilon}^{e} + \boldsymbol{\varepsilon}^{vp} \tag{1}$$

The anisotropy is regarded by structural tensors and not by symmetry conditions based on a reference coordinate system. The so called structural tensors represent the material symmetries of the respective anisotropy class as an intrinsic material property. They are used as additional arguments in the constitutive equations. This enables a coordinate system free representation of the anisotropic material laws as isotropic tensor functions. Moreover, finite fiber rotations can be regarded easily. The structural tensor $\mathbf{A}$ which represents the symmetry conditions of transversely isotropic materials is defined by the dyadic product of the unit vector of the preferred direction:

$$\mathbf{A} = \mathbf{a}\otimes\mathbf{a} \;\rightarrow\; A_{ij} = a_i a_j. \tag{2}$$

The structural tensor is used as an additional argument in order to formulate the elastic free energy density, the yield function and the plastic potential formulation [3]. The elastic free energy density for the transversely isotropic model reads:

$$\Psi(\boldsymbol{\varepsilon}, \mathbf{A}) = \frac{1}{2}\lambda(\mathrm{tr}\boldsymbol{\varepsilon})^2 + \mu_T \mathrm{tr}(\boldsymbol{\varepsilon})^2 + \alpha(\mathbf{a}\boldsymbol{\varepsilon}\mathbf{a})\mathrm{tr}(\boldsymbol{\varepsilon}) + 2(\mu_L - \mu_T)(\mathbf{a}\boldsymbol{\varepsilon}^2\mathbf{a}) + \frac{1}{2}\beta(\mathbf{a}\boldsymbol{\varepsilon}\mathbf{a})^2, \tag{3}$$

with the five elasticity constants λ, μ_T, μ_L, α, β as invariant coefficients. The conversion into engineering constants and vice versa can be found in [3]. The stress ($\boldsymbol{\sigma}$) and the elasticity tensor ($\mathbb{C}_e$) can be obtained by computing the first and the second derivatives of the free energy density with respect to the strain tensor, respectively:

$$\boldsymbol{\sigma} = \partial_{\boldsymbol{\varepsilon}}\Psi(\boldsymbol{\varepsilon}, \mathbf{A}); \quad \mathbb{C}_e = \partial^2_{\boldsymbol{\varepsilon}}\Psi(\boldsymbol{\varepsilon}, \mathbf{A}) \tag{4}$$

In order to formulate the transversely isotropic invariants used in the yield surface formulation, a decomposition of the stress in plasticity inducing stresses and elastic reaction stresses is assumed:

$$\boldsymbol{\sigma} = \boldsymbol{\sigma}^{\mathrm{reac}} + \boldsymbol{\sigma}^{\mathrm{pind}} \tag{5}$$

With the elastic reaction and plasticity inducing stresses defined as:

$$\begin{aligned}\sigma^{\text{reac}} &= \frac{1}{2}(\text{tr}\boldsymbol{\sigma} - \mathbf{a}\boldsymbol{\sigma}\mathbf{a})\mathbf{1} - \frac{1}{2}(\text{tr}\boldsymbol{\sigma} - 3\mathbf{a}\boldsymbol{\sigma}\mathbf{a})\mathbf{A} \\ \sigma^{\text{pind}} &= \boldsymbol{\sigma} - \frac{1}{2}(\text{tr}\boldsymbol{\sigma} - \mathbf{a}\boldsymbol{\sigma}\mathbf{a})\mathbf{1} + \frac{1}{2}(\text{tr}\boldsymbol{\sigma} - 3\mathbf{a}\boldsymbol{\sigma}\mathbf{a})\mathbf{A}\end{aligned} \tag{6}$$

The set of invariants used to formulate the yield surface reads [3]:

$$\begin{aligned}\mathrm{I}_1 &= \tfrac{1}{2}\text{tr}\left(\boldsymbol{\sigma}^{\text{pind}}\right)^2 - \mathbf{a}\left(\boldsymbol{\sigma}^{\text{pind}}\right)^2\mathbf{a}, \\ \mathrm{I}_2 &= \mathbf{a}\left(\boldsymbol{\sigma}^{\text{pind}}\right)^2\mathbf{a}, \\ \mathrm{I}_3 &= \text{tr}(\boldsymbol{\sigma}) - \mathbf{a}\boldsymbol{\sigma}\mathbf{a}\end{aligned} \tag{7}$$

With the invariants defined in (7), the transversely isotropic yield surface for UD composites reads [3]:

$$\mathrm{f}(\boldsymbol{\sigma}, \bar{\varepsilon}^{\text{vp}}, \mathbf{A}) = \alpha_1\mathrm{I}_1 + \alpha_2\mathrm{I}_2 + \alpha_3\mathrm{I}_3 + \alpha_{32}\mathrm{I}_3^2 + \alpha_4\mathrm{I}_4 + \alpha_{42}\mathrm{I}_4^2 - 1 \leq 0,$$

with

$$\begin{aligned}\alpha_3 = \alpha_3^t, \alpha_{32} = \alpha_{32}^{\text{t}} \text{ if } \mathrm{I}_3 > 0 \quad \text{and} \\ \alpha_3 = \alpha_3^c, \alpha_{32} = \alpha_{32}^{\text{c}} \text{ if } \mathrm{I}_3 \leq 0.\end{aligned} \tag{8}$$

The proposed yield function results in 6 yield surface parameters that have to be determined. Each one of these parameters and the corresponding invariants are related to certain loading states: transverse shear, in-plane shear, uniaxial and biaxial transverse tension and uniaxial and biaxial transverse compression. Figure 4 shows a schematic representation of the transversely isotropic yield surface in stress space. The highlighted points are the ”trigger points” of the yield surface, in which yielding is controlled. That is, in each of these points, an initial yield stress and a hardening curve giving the yield stress vs. the corresponding plastic strain is regarded via tabulated data. Consequently, the yield surface parameters $\alpha(..)$ are a function of the equivalent plastic strain. This is explained in detail in [3].

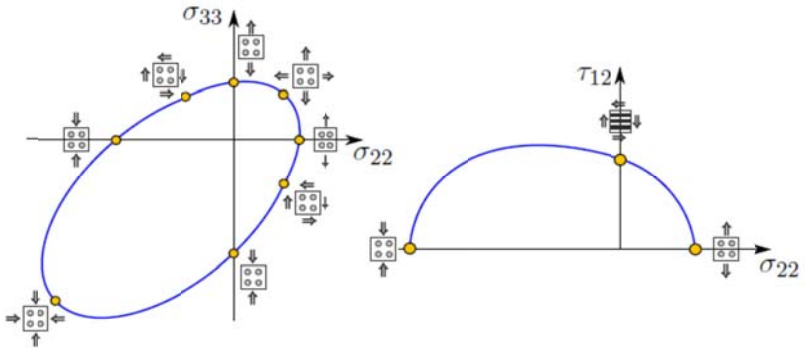

Figure 4. Schematic representation of the yield surface for UD composites in stress space.

The evolution of the viscoplastic strains reads:

$$\dot{\boldsymbol{\varepsilon}}^{\text{vp}} = \frac{\langle \mathrm{f}(\boldsymbol{\sigma}, \bar{\varepsilon}^{\text{vp}}, \mathbf{A})\rangle^{\text{m}}}{\eta}\mathbf{n}_{\text{g}}, \tag{9}$$

with the two viscoplastic parameters η and m.

6. Model Validation

A linear elastic behaviour until fracture is observed for uniaxial transverse tension (Figure 5a). Nonlinearity in transverse tension must be defined however to trigger the nonlinear behaviour for combined shear-tensile stress states (15°, 30°, 45° off-axis tests). A hypothetic tensile hardening curve (Figure 5b) was derived, using a data reduction procedure for the plasticity model proposed by [7]. The shear hardening curve was taken from [2].

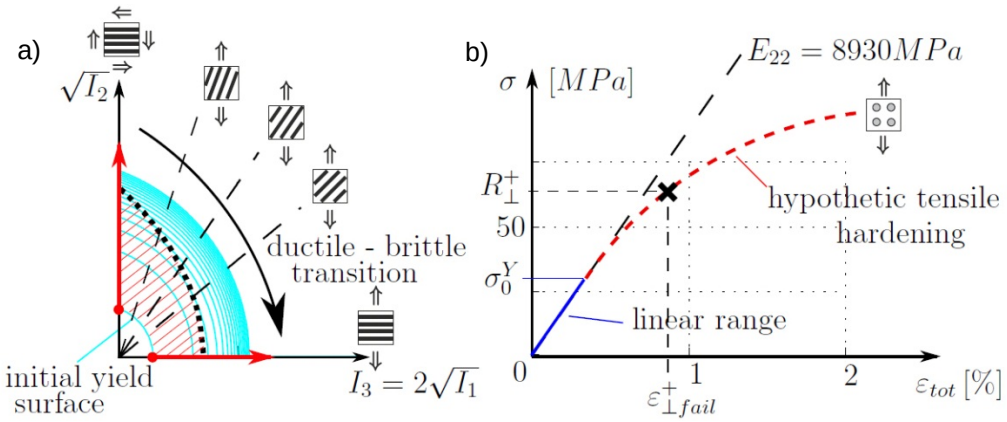

Figure 5. Transition from ductile to brittle response and nonlinear stress-strain curve for transverse tension.

Figure 6 shows the measured and simulated static and dynamic axial stress-strain curves. For the 15° and 30° specimen type, the comparison between experiment and simulation is excellent. Further experimental data is however required for a better comparison in case of the 45° off-axis and the 90° specimen. It is noted that the model correctly predicts failure under static loading, using an invariant based failure criterion [8]. The simulated dynamic stress-strain curves were truncated since the failure criterion is not yet strain rate dependent.

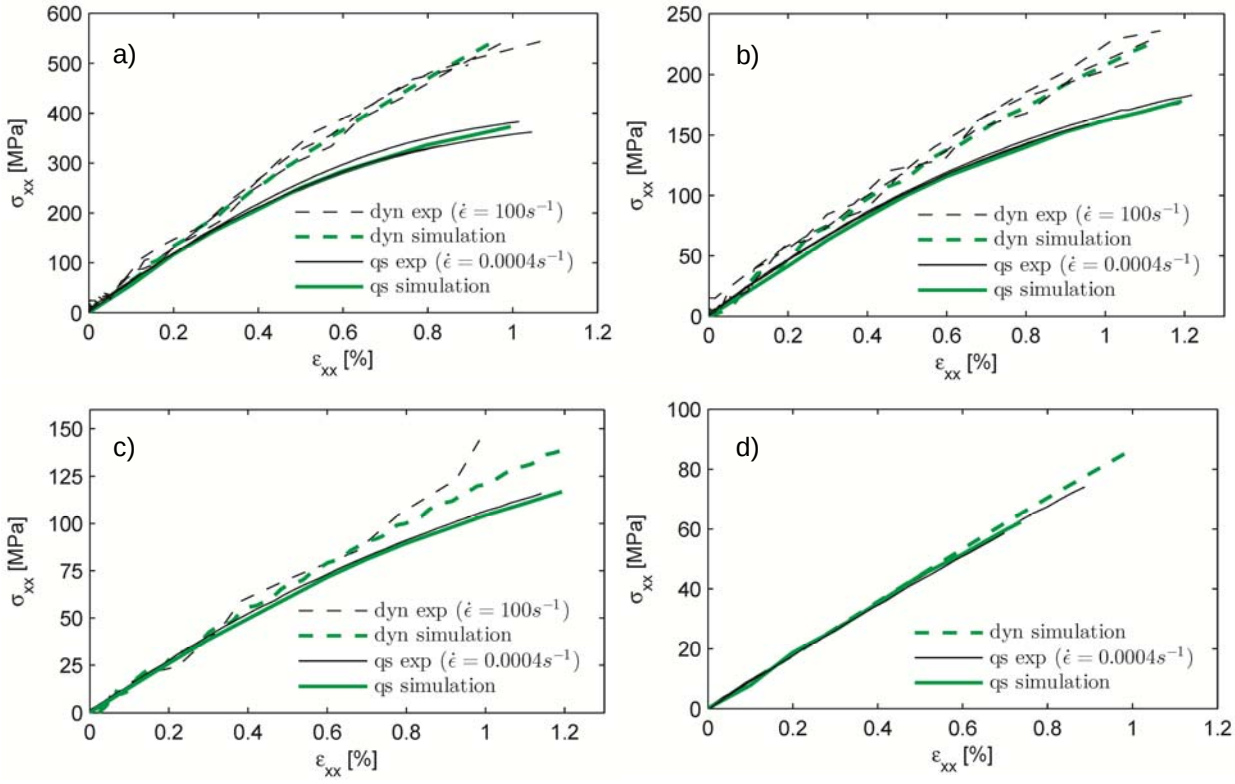

Figure 6. Quasi-static and dynamic axial stress-strain response for: (a) 15° off-axis tension, (b) 30° off-axis tension, (c) 45° off-axis tension and (d) 90° transverse tension.

7. Summary and Conclusion

The mechanical response of IM7-8552 was investigated for transverse tension and transverse tension / in-plane shear loading at static and dynamic (100 s^{-1}) strain rates. A shift from nonlinear to predominantly linear stress-strain response was observed for the dynamic off-axis tests, whereas the response for transverse tension is already linear under static loading. The nonlinearity observed for transverse compression [2], is truncated by the low transverse tensile strength. The measured axial strengths increased by 47%, 30% and 24% for the 15°, 30° and 45° off-axis specimens. The decreasing rate effect on the axial strengths can be attributed to a decreasing strain rate with increasing off-axis angle when considering the strain rate acting in the fracture plane of the respective specimen type. From the measured axial strengths the failure envelope for combined transverse tension / in-plane shear loading was derived for both strain rate levels and compared with the Puck IFF Mode A failure criterion. For the static strain rate a good correlation was observed between experimental and predicted failure envelope. Due to the constant strength increase of 40% assumed for the dynamic failure criterion, the experimental and predicted envelope derivate with increasing off-axis angle. Further dynamic tests at constant strain rates acting in the failure plane are therefore needed to better understand the strain rate effect for the combined tension-shear stress state.

Together with a previously published experimental study on the mechanical response of IM7-8552 under transverse compression and combined transverse compression / in-plane shear loading at static and dynamic strain rates [2] a comprehensive data set now exists regarding the strain rate dependent mechanical behaviour of this composite material system.

The herein presented axial stress-strain response, measured for the transverse tension and off-axis tension tests, was simulated using a fully 3D transversely isotropic elastic-viscoplastic constitutive model, able to predict nonlinearities under multi-axial loading conditions prior to the onset of cracking [3]. A very good correlation between the measured and numerically predicted stress-strain response was achieved for all specimen types and strain rate levels.

References

[1] N. Taniguchi, T. Nishiwaki, N. Hirayama, H. Nishida and H. Kawada. Dynamic tensile properties of carbon fiber composite based on thermoplastic epoxy resin loaded in matrix-dominant directions. *Composites Science and Technology*, 69:207-213, 2009.

[2] H. Koerber, J. Xavier and P.P. Camanho. High strain rate characterisation of unidirectional carbon-epoxy IM7-8552 in transverse compression and in-plane shear using digital image correlation. *Mechanics of Materials*, 42:1004-1019, 2010.

[3] M. Vogler, R. Rolfes and P.P. Camanho. Modeling the inelastic deformation and fracture of polymer composites–part I: plasticity model. *Mechanics of Materials*, 59:50-64, 2013.

[4] R. Gerlach, C. Kettenbeil and N. Petrinic. A new split Hopkinson tensile bar design. *International Journal of Impact Engineering*, 50:63-67, 2012.

[5] H. Koerber and P.P. Camanho. High strain rate characterisation of unidirectional carbon-epoxy IM7-8552 in longitudinal compression. *Composites Part A*, 42:462-470, 2011.

[6] A. Puck, H. Schürmann. Failure analysis of FRP laminates by means of physically based phenomenological models. *Composites Science and Technology*, 58:1045-1067, 1998.

[7] C.T. Sun and J.L. Chen. A simple flow rule for characterizing nonlinear behaviour of fiber composites. *Journal of Composite Materials*, 23:1009-1020, 1989.

[8] M. Vogler, G. Ernst and R. Rolfes. Invariant based transversely-isotropic material and failure model for fiber-reinforced polymers. *Computers, Materials & Continua*, 16: 25-49, 2010.